A Microstructure Study on an AZ31 Magnesium Alloy Tube after Hot Metal Gas Forming Process

Yi Liu and Xin Wu

An AZ31 magnesium alloy tube has been deformed by the hot metal gas forming (HMGF) technique. Microstructures before and after deformation have been investigated by using Electron Backscattered Diffraction (EBSD) and Electron Microscopy. Due to the inhomogeneous distribution by induction heating, there is a temperature gradient distribution along the tube axis. Accordingly, the deformation mechanism is also different. In the middle area of deformation zone where the temperature is ~410 °C, almost no twinning has been found, whereas at the edge areas of deformation zone where the temperature is ~200 °C, a high density of twins has been found. EBSD experiments show a weak (0001) fiber texture along the radial direction of the tube before and after deformation in the high-temperature zone. EBSD experiments on the low temperature deformation region were not successful due to the high stored energy. Schmid factor analysis on the EBSD data shows that, despite the (0001) fiber texture, there are still many grains favoring basal slip along both the axis direction and hoop direction.

1. Introduction

Magnesium alloys have received a great deal of attention from the automobile industry in recent years because of their light weight, high-specific strength (Ref 1, 2), and recycle ability (Ref 3). As a "near zero fabrication" process, in addition to casting, forming is often preferred to make certain auto parts with magnesium alloys. In recent years, the hot metal gas forming (HMGF) technique has been developed (Ref 4, 5) under the funding support from NIST-ATP and 17 joint venture member companies, and later from General Motor Corporation. Tubes of several engineering metals including steels, aluminum, and magnesium alloys have been tested by this technique (Ref 6). In these tests, induction heating was used at the location where deformation was needed and the tube was deformed by introducing a compressive gas into the tube.

It has been well demonstrated that both fine-grained and coarse-grained magnesium alloys exhibit very good plasticity at elevated temperatures although they have less plasticity at room temperature because of the lack of slip systems at low temperature (Ref 6-17). Different deformation mechanisms

are required in each material. Fine-grained Mg alloys need grain boundary sliding while coarse-grained Mg alloys need the activation of slip systems. Previous work by the present authors show that different deformation mechanisms can be identified from texture evolution observed with Electron-Backscattered Diffraction (EBSD) studies on fine-grained (Ref 18) and coarse-grained AZ31 Mg alloys (Ref 19). In the fine-grained AZ31 Mg alloy with the initial grain size less than 21 μm, both grain boundary sliding and slip were observed. The strong pre-existing (0001) fiber texture was almost unchanged during entire deformation until fracture (over 500% elongation at 500 °C) and the (0001) fiber texture was not destroyed due to grain boundary sliding (Ref 18). This phenomenon suggests a "directional" grain boundary sliding and non-basal slip during deformation since the basal slip was not favored with the initial strong (0001) fiber texture. In the coarse-grained AZ31 Mg alloy, with the initial grain size larger than 100 μm, on the other hand, the pre-existing weak (0001) fiber texture evolved into a strong texture which is close to $\{0001\}$ $\langle 1\bar{1}00 \rangle$, and [0001] directions of grains rotated towards the orientation perpendicular to the tension axis of the samples (Ref 19). This phenomenon strongly suggests that basal slip is the main slip mode during deformation.

Based on the above studies, it would be very interesting to study the texture evolution of AZ31 Mg alloy tube during HMGF process and the preliminary results will be presented in this paper.

2. Experimental Details

An AZ31 alloy tube was selected to conduct the experiments. The Mg tube was produced by hot-extrusion at a laboratory scale at Berlin Technological University, Germany with the chemical composition given as: Al: 2.5-3.5%, Zn: 0.5-1.5%, Mn: 0.05-0.4%, Si: 0.1%, Cu: 0.1%, Ni: 0.005%, Mg: Balance. It can be seen that some elements are in wide ranges.

Yi Liu, Laboratory of Analytical Electron Microscopy, Central Instrument Facility, Department of Chemistry, Wayne State University, 5101 Cass Avenue, Detroit, MI 48202; Contact e-mail: yliu@chem.wayne.edu. **Xin Wu,** Department of Mechanical Engineering and Institute for Manufacturing Research, Wayne State University, 5050 Anthony Wayne Drive, Detroit, MI 48202.

However, no accurate chemical composition was available. In this paper, we used samples from the different locations of a single tube after HMGF process. Thus, the wide variation of the raw material batch has no effect on the comparison of microstructures produced at different temperatures and strains. The as-received Mg alloy tube is 42.4 mm in diameter (1.6 in) and 2 mm in wall thickness. The HMGF test was conducted by using a tube biaxial formability test described in Ref (6). During the test, the tube specimen was rapidly heated to the desired temperature in about 100 s using an induction-heating unit. The maximum temperature at the length center of the induction coil (location A in Fig. 1) was monitored to be about 410 °C by a K type thermocouple contacting directly to the tube. Nitrogen gas at 0.88 MPa (or 128 psi) pressure was supplied inside the tube. The temperature at location B was not monitored. However, a separate study of temperature measurement on the tube was performed with 24 thermocouples along three lines. The lines are parallel to the tube axis and are separated by 90° along the hoop direction of the tube. The thermocouples are separated with 1″ spacing in each line. A temperature distribution similar to a sinusoidal waveform was found. Based on this study, the temperature at location B was roughly estimated as about 200 °C.

Samples were cut from different locations labeled as "A", "B" and "C" from the tube as shown in Fig. 1. The axial, radial and hoop directions of the tube are defined as X, Y and Z directions, respectively. The strains in the samples were estimated by simply measuring the pre-etched circle grid on the tube before and after deformation. The maximum effective true strain was measured as 0.35 in sample A, which was at about 410 °C. The average strain rate was calculated as 0.005/s by dividing the total effective strain by the total forming time. The effective true strain in sample B was measured as 0.14 in the same way as sample A at about 200 °C. Sample C represents the non-deformed state of the Mg alloy tube.

The Z planes of the samples were mechanically ground and polished by standard methods including polishing with 0.05 μm Colloidal Silica suspension. The samples were then finally electro-polished using an electrolyte of 20% nitric acid in methanol at room temperature. The voltage was controlled at 2 V. The samples for SEM observations were etched by a solution of 5 mL acetic acid, 6 g picric acid, 10 mL distilled water, and 100 mL ethanol. EBSD experiments were conducted in a Hitachi S-2400 scanning electron microscope (SEM) equipped with an Orientation Imaging Microscopy (OIM) system made by HKL Technology, Denmark (now merged into Oxford Instrument). The SEM was operated at 25 kV. The working distance was adjusted to 15 mm. The beam current was 90-115 μA. To obtain stronger EBSD signals from the surface of the Mg alloy samples, the current of condenser lens was decreased to increase beam intensity illuminating the samples sacrificing resolution to some extent. This is the so-called "high probe current mode" which is very important for EBSD analysis. Figure 2 shows an example of EBSD pattern obtained from the current Mg alloy tube.

3. Results and Discussions

Microstructural observations, as shown in Fig. 3, indicate that there is a high density of twins in the as-received AZ31 magnesium alloy tube (Sample C), especially in the areas near the tube surface (Fig. 3a and c). The twinning is probably related to the extrusion process of the tube at relatively high strain rate and low temperature (no information is available). The intercept length of the grain size was measured to be 31 μm, which corresponds to a mean grain size of 54 μm.

Figure 4 shows the microstructures of sample A (Fig. 4a) and Sample B (Fig. 4b). It is interesting to find that there is
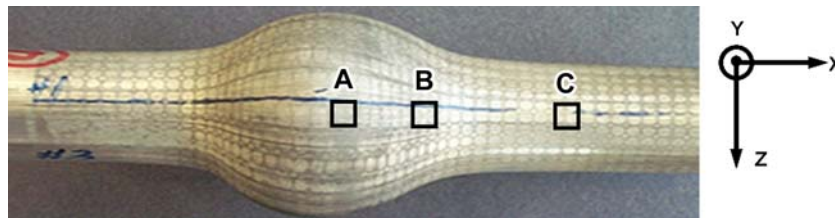

Fig. 1 AZ31 Magnesium alloy tube after hot metal gas forming
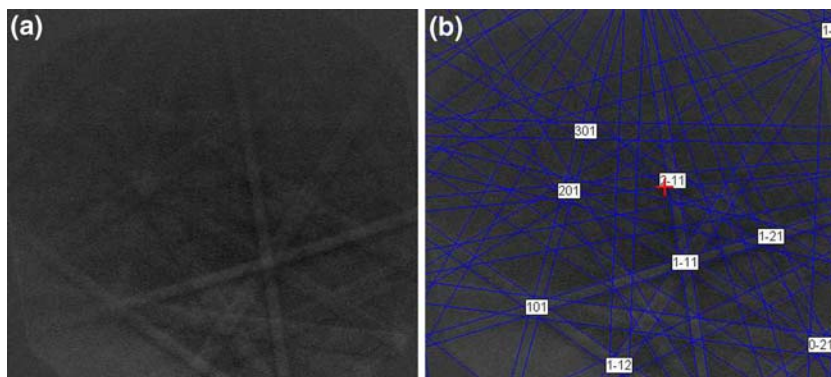

Fig. 2 An example of EBSD pattern and its indexation obtained from the current AZ31 Mg alloy tube

almost no twining in sample A, which represents the area deformed at ~410 °C, while a high density of twins can be found in sample B, which corresponds to the area deformed at ~200 °C. The intercept length of the grain size was measured to be 31.62 μm in sample A and 33 μm in sample B, which corresponds to grain sizes of 55 and 57 μm, respectively. It is thus very clear that the grain size of the Mg alloy tube remained almost the same during deformation. Voids were also found in the deformed area as indicated by arrows in Fig 4a. No voids were found in sample C, which was cut from the undeformed area as shown in Fig. 3.

EBSD experiments were performed for samples A, B, and C. However, only samples A and C were able to generate diffraction patterns. No clear and solvable pattern could be obtained from sample B, most probably due to the high residual strain in the sample caused by the deformation at low temperature (~200 °C). In sample A, which represents the area of deformation at about 410 °C, 76% of patterns were solved (also called hit rate), while in sample C which represents the undeformed area of the tube, 54% patterns were solved. In general, there are several reasons responsible for unclear or unsolvable patterns: (i) the surface of the sample is not prepared very well so that a strained layer from grinding and polishing may still exist on the surface; (ii) the beam hits the imperfections on the surface, such as etching pitches, dirts, voids, etc.; (iii) the beam hits grain boundaries or the triple junction points of grain boundaries where several sets of EBSD patterns overlap; and (iv) high residual strain energy is stored in the sample. But in the current experiments, among these reasons, it is believed that the high residual strain energy may be more responsible for the unclear and unsolvable patterns, especially for sample B deformed at low temperature. Sample A was deformed at higher temperature, so the hit rate of EBSD experiment is higher than sample C. However, since those zero solution patterns will not contribute to the statistical analysis of texture, low hit rate EBSD experiments still make sense for texture analysis if the area analyzed is large enough. Figure 5 shows TEM observations on samples deformed at ~410 °C (Fig. 5a) and sample B deformed at ~200 °C (Fig. 5b). A higher density of dislocations can be found in sample B than in sample A.
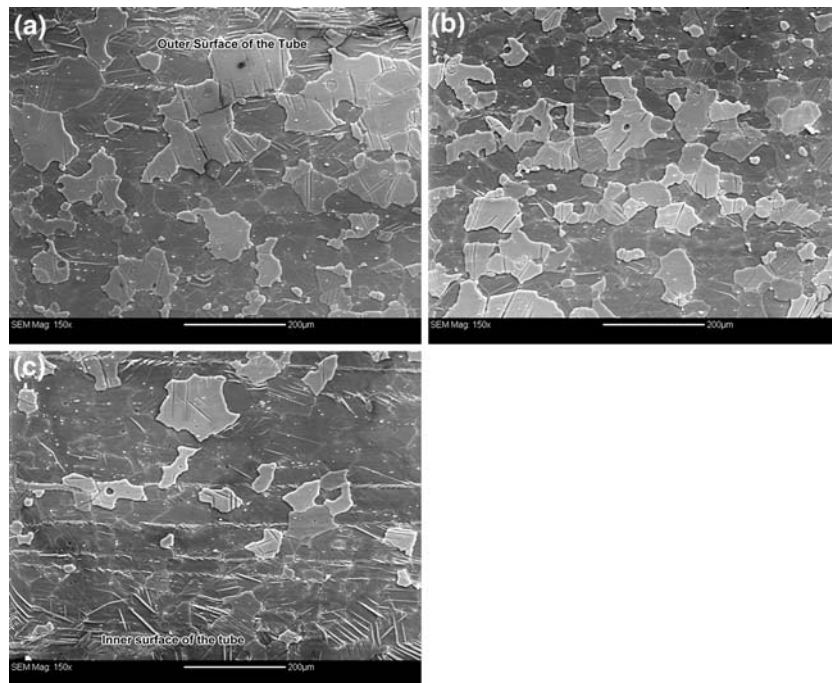

Fig. 3 Microstructure along the wall thickness direction in the undeformed area (as-received) of AZ31 Mg tube. (**a**) Near out-surface, (**b**) at middle position, and (**c**) near inner-surface
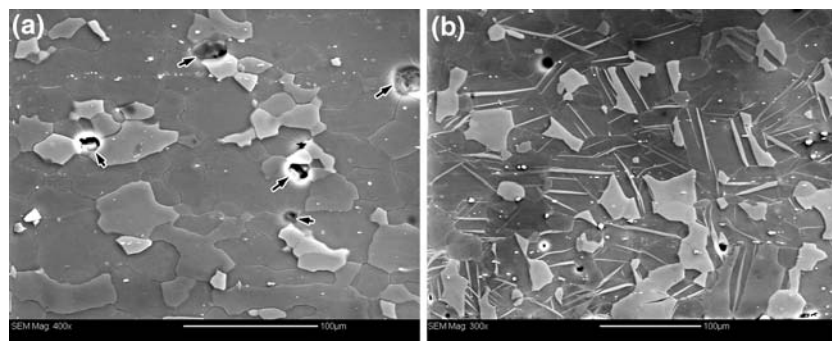

Fig. 4 Microstructure along the wall thickness direction in the deformed area of AZ31 Mg tube. (**a**) Sample A and (**b**) Sample B

Figure 6 shows pole figures obtained from EBSD data of both the undeformed area in sample C (Fig. 6a) and deformed area in sample A (Fig. 6b) of the Mg alloy tube. A weak (0001) fiber texture pre-existing in the undeformed area was detected along *Y* direction, which is the radial direction of the tube (Fig. 6a). Deformation did not change the texture as indicated by Fig. 6b. This is probably because the strain is still low (0.35 true strains). The pre-existing (0001) fiber texture along radial direction is due to the extrusion process used to make the tube, during which the (0001) basal planes tend to be parallel to the extrusion direction of the tube because of the basal slip. The formation of (0001) fiber texture is similar to Mg alloy plate or sheet by rolling process.

Figure 7 shows OIM mapping on an area of 300×200 μm in sample A with a step size of 1 μm. Figure 7a shows the raw OIM data. It can be seen that some points are unsolved. The hit
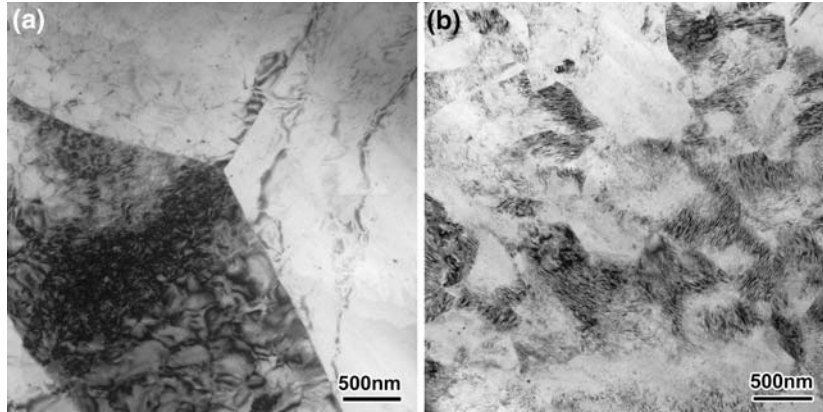

Fig. 5 High-density dislocations in (**a**) sample A deformed at ~450 °C, and (**b**) sample B deformed at ~200 °C of AZ31 Mg alloy tube
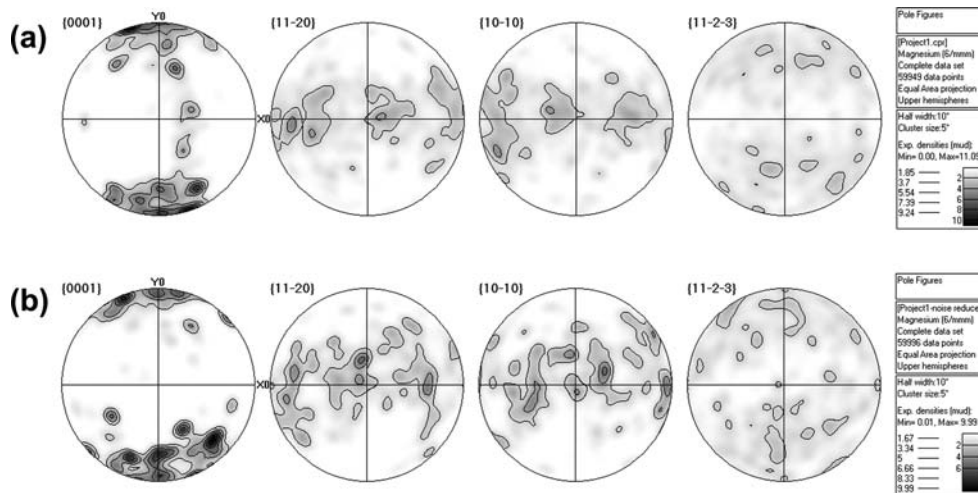

Fig. 6 Pole figures corresponding to (**a**) undeformed area (sample C) and (**b**) deformed area (sample A) of the AZ31 Mg alloy tube
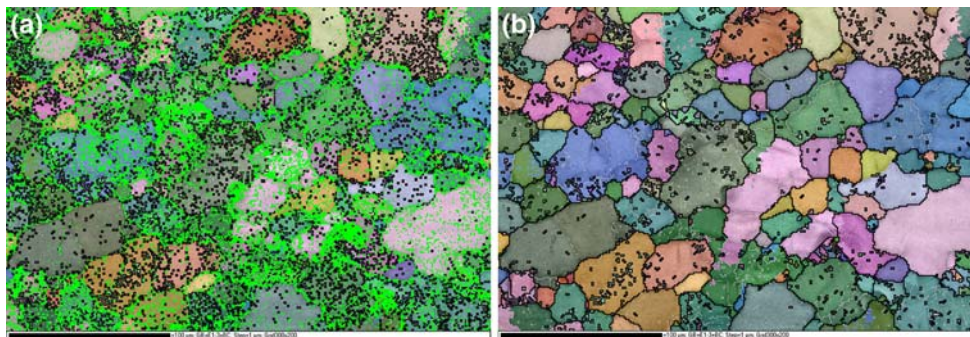

Fig. 7 OIM mapping on an area of 300×200 μm in the deformed area (sample A) with step size 1 μm. (**a**) OIM raw data, (**b**) noise reduced OIM by HKL software
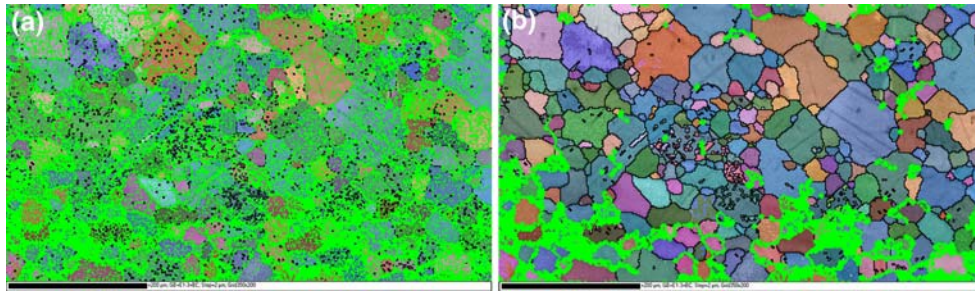
Fig. 8 OIM mapping on an area of 700×400 μm in the undeformed area (sample C) with step size 2 μm. (**a**) OIM raw data and (**b**) noise reduced OIM by HKL software
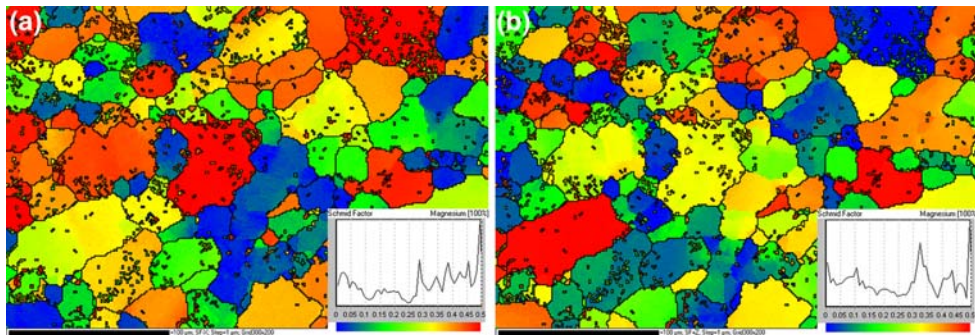

Fig. 9 (**a**) OIM based on Schmid Factor of basal slip showing potential grains for deformation (**a**) along the axis direction (X), and (**b**) along the hoop direction (Z) of the tube. The insets show distribution of grains favored to basal slip

rate is 76%. By using the EBSD (HKL) software, most of those unsolved points can be assigned to their solved neighborhoods. In this way, the "noise" of the raw data can be reduced as shown in Fig. 7b. It is found that Fig. 7b represents the real situation.

Same situation occurred in sample C. Figure 8 shows OIM mapping on an area of 700×400 μm in sample C with a step size of 2 μm. Figure 8a shows the raw OIM data and Fig. 8b shows the "noise" reduced data. The hit rate is 54% as mentioned before. It can be seen that OIM was unable to identify twins found in the sample (Fig. 8b). This is probably due to the fact that sample C contains more stored energy than sample A and more points were not solvable than those in sample A. However, the noise filtered OIM shown in Fig. 8b is still very close to the real situation.

Figure 9 shows OIM of Schmid Factor for basal slip along the tube axial direction (X) (Fig. 7a) and the hoop direction (Z) (Fig. 7b) of the same area as shown in Fig. 7 in sample A of the tube. The insets show the distribution of grains favored to basal slip. It can be found that, there are still many grains favoring basal slip after deformation although there is a pre-existing weak (0001) fiber texture in the tube.

4. Conclusions

An AZ31 magnesium alloy tube was deformed using HMGF technique. The deformation temperature and strain varies along the tube longitudinal direction; accordingly, the deformation mechanism is also different. In the area of the tube near center of the induction coil where the temperature was

~410 °C, almost no twining has been found, whereas near the coil edge, where the temperature was ~200 °C, a high density of twins has been found. EBSD experiments show a weak (0001) fiber texture in the sample before and after deformation. And even though there is a pre-existing (0001) fiber texture, there are still many grains favorably aligned for basal slip along both the axial and the hoop directions.

References

1. A.A. Luo, Magnesium: Current and Potential Automotive Applications, *JOM*, 2002, **54**(2), p 42–48
2. A.A. Luo, Recent Magnesium Alloy Development for Automotive Powertrain Applications, *Mater. Sci. Forum*, 2003, **419–4**, p 57–65
3. L. Riopelle, Recycling of Magnesium Makes Cents, *JOM*, 1996, **48**(10), p 44–46
4. B. Dykstra, G. D. Pfafffmann, and X. Wu, *SAE Technical Paper Series*, 1999, Sept 28–30
5. G. D. Pfaffmann, X. Wu, and W. K. Dykstra, Hot Metal Gas Forming of Auto Parts?, *Adv. Mater. Process.*, 2000, p H35–37
6. X. Wu, H. Hao, Y. Liu, F. Zhu, J. Jiang, R. Krishnamurthy, S. Wang, P.E. Smith, W. Bland, and G.D. Pfaffmann, Elevated Temperature Formability of Some Engineering Metals for Gas Forming of Automotive Structures, *J. Mater. Manufact. SAE Trans.*, 2001, **110**(5), p 1045–1056

7. M. Mabuchi, K. Ameyama, H. Iwasaki, and K. Higashi, Low Temperature Superplasticity of AZ91 Magnesium Alloy with Non-equilibrium Grain Boundaries, *Acta Mater.*, 1999, **47**(7), p 2047–2057

8. H. Watanabe, T. Mukai, and K. Higashi, Superplasticity in a ZK60 Magnesium Alloy at Low Temperatures, *Scripta Mater.*, 1999, **40**(4), p 477–484

9. X. Wu and Y. Liu, Superplasticity of Coarse-grained Magnesium Alloy, *Scripta Mater.*, 2002, **46**(4), p 269–274

10. X. Wu, Y. Liu, and H.Q. Hao, High Strain Rate Superplasticity and Microstructure Study of a Magnesium Alloy, *Superplast. Adv. Mater., ICSAM-2000*, 2001, **357–3**, p 363–368

11. T. Mohri, M. Mabuchi, M. Nakamura, T. Asahina, H. Iwasaki, T. Aizawa, and K. Higashi, Microstructural Evolution and Superplasticity of Rolled Mg-9Al-1Zn, *Mater. Sci. Eng. A*, 2000, **290**(1–2), p 139–144

12. T.G. Nieh and J. Wadsworth, Superplasticity in a Powder-Metallurgy Magnesium Composite, *Scripta Metall. Mater.*, 1995, **32**(8), p 1133–1137

13. J.C. Tan and M.J. Tan, Superplasticity in a Rolled Mg-3A1-1Zn alloy by Two-stage Deformation Method, *Scripta Mater.*, 2002, **47**(2), p 101–106

14. J.C. Tan and M.J. Tan, Superplasticity and Grain Boundary Sliding Characteristics in Two Stage Deformation of Mg-3Al-lZn Alloy Sheet, *Mat. Sci. Eng. A Struct.*, 2003, **339**(1–2), p 81–89

15. J.C. Tan and M.J. Tan, Dynamic Continuous Recrystallization Characteristics in Two Stage Deformation of Mg-3A1-lZn Alloy Sheet, *Mat. Sci. Eng. A Struct.*, 2003, **339**(1–2), p 124–132

16. S.R. Agnew, J.A. Horton, and M.H. Yoo, Transmission Electron Microscopy Investigation of <c+a> Dislocations in Mg and Alpha-solid Solution Mg-Li Alloys, *Metal. Mater. Trans. A Phys. Metall. Mater. Sci.*, 2002, **33**(3), p 851–858

17. S.R. Agnew and O. Duygulu, A Mechanistic Understanding of the Formability of Magnesium: Examining the Role of Temperature on the Deformation Mechanisms, *Magnesium Alloys 2003, Pts 1 and 2*, 2003, **419–4**, p 177–188

18. Y. Liu and X. Wu, *Magnesium Technology 2005, TMS (The Minerals, Metals & Materials Society), 2005*, H.I. Kaplan and B. R. Powell, N. R. Neelamegghams, Eds., San Francisco, California, 2005

19. Y. Liu and X. Wu, An Electron-Backscattered Diffraction Study of the Texture Evolution in a Coarse-grained AZ31 Magnesium Alloy Deformed in Tension at Elevated Temperature, *Metall. Mater. Trans. A*, 2006, **37A**(Jan), p 7–17 (January)